Lermusiaux, P.F.J. et al., 2024. Real-time Ocean Probabilistic Forecasts, Reachability Analysis, and Adaptive Sampling in the Gulf of Mexico. In: OCEANS '24 IEEE/MTS Halifax, 23–26 September 2024, in press.

Real-time Ocean Probabilistic Forecasts, Reachability Analysis, and Adaptive Sampling in the Gulf of Mexico

P.F.J. Lermusiaux[a,†], P.J. Haley, Jr.[a], C. Mirabito[a], E.M. Mule[a], S.F. DiMarco[b], A. Dancer[b], X. Ge[b], A.H. Knap[b], Y. Liu[b], S. Mahmud[b], U.C. Nwankwo[b], S. Glenn[c], T.N. Miles[c], D. Aragon[c], K. Coleman[c], M. Smith[c], M. Leber[d], R. Ramos[d], J. Storie[d], G. Stuart[e], J. Marble[e], P. Barros[e], E.P. Chassignet[f], A. Bower[g], H.H. Furey[g], B. Jaimes de la Cruz[h], L.K. Shay[h], M. Tenreiro[i], E. Pallas Sanz[i], J. Sheinbaum[i], P. Perez-Brunius[i], D. Wilson[j], J. van Smirren[k], R. Monreal-Jiménez[l], D.A. Salas-de-León[l], V.K. Contreras Tereza[m], M. Feldman[n], and M. Khadka[n]

[a]*Department of Mechanical Engineering, Massachusetts Institute of Technology, Cambridge, MA*

[b]*Department of Oceanography, Texas A&M University*, [c]*Department of Marine and Coastal Sciences, Rutgers University*

[d]*Woods Hole Group, Inc.*, [e]*Fugro*, [f]*Department of Earth, Ocean and Atmospheric Science, Florida State University*

[g]*Physical Oceanography, Woods Hole Oceanographic Institution*

[h]*Rosenstiel School of Marine, Atmospheric, and Earth Science, University of Miami*

[i]*Department of Oceanography, CICESE*, [j]*University of the Virgin Islands*, [k]*Ocean Sierra*

[l]*Universidad Nacional Autónoma de México*, [m]*Mexican Institute of Water Technology*, [n]*Gulf Research Program, NASEM*

[†]Corresponding author: pierrel@mit.edu

***Abstract*—The first steps towards integrating autonomous monitoring, probabilistic forecasting, reachability analysis, and adaptive sampling for the Gulf of Mexico were demonstrated in real-time during the collaborative Mini-Adaptive Sampling Test Run (MASTR) ocean experiment, which took place from February to April 2024. The emphasis of this contribution is on the use of the MIT Multidisciplinary Simulation, Estimation, and Assimilation Systems (MSEAS) including Error Subspace Statistical Estimation (ESSE) large-ensemble forecasting and path planning systems to predict ocean fields and uncertainties, forecast reachable sets and optimal paths for gliders, and guide sampling aircraft and ocean vehicles toward the most informative observations. Deterministic and probabilistic ocean forecasts are exemplified and linked to the variability of the Loop Current (LC) and LC Eddies, demonstrating predictive skill by real-time comparisons to independent data. Risk forecasts in terms of probabilities of currents exceeding 1.5 kt were provided. The most informative sampling patterns for Remote Ocean Current Imaging System (ROCIS) flights were forecast using mutual information between surface currents and density anomaly. Finally, we guided four underwater gliders using probabilistic reachability and path-planning forecasts.**

***Index Terms*—Ocean modeling, probabilistic forecasting, predictability, forecast skill, data assimilation, path planning, adaptive sampling, mutual information, ocean gliders, aircraft.**

I. Introduction

The integration of novel autonomous ocean monitoring and probabilistic ocean forecasting can be most beneficial to the Gulf of Mexico (GoM) and its communities and stakeholders. Such integration combines systems for high-resolution stochastic ocean modeling, multi-platform autonomous observing, data assimilation, path planning, adaptive sampling, real-time operations, and of course human interactions. The first steps towards this integration for the GoM were demonstrated in real-time during the collaborative Mini-Adaptive Sampling Test Run (MASTR) ocean experiment [1, 2]. The main MASTR effort occurred from February to April 2024, as part of the collaborative "Understanding Gulf Ocean Systems (UGOS-3)" initiative sponsored by the Gulf Research Program of the U.S. National Academies of Sciences, Engineering, and Medicine. The emphasis of the present contribution is on some of the real-time MASTR results. They include large-ensemble forecasting of physical ocean fields, uncertainties, and risks, predicting reachable regions and optimal paths for aircraft and marine platforms, forecasting optimal ocean sampling times and locations, and evaluating the skill of forecasts by comparison with observations.

The overall oceanographic state in the GoM is directly linked to the dynamics and state of the Loop Current (LC) [3–7]. The LC is a warm-water current that flows northward from the Caribbean Sea, enters into the GoM, and exits through the Florida Strait. The degree to which the LC penetrates the GoM is intermittent and variable on multiple timescales. The northernmost extent of the penetration has a range of $24°$N to $28°$N [8–12]. This penetration has been observed to have a bimodal distribution [8, 11, 13–20]. The major mode of this distribution is centered on $26.5°$N to $26.75°$N, with the minor mode centered on $24.5°$N to $24.75°$N. The horizontal extent of the LC in the GoM is also intermittent, but has been observed to exhibit quasi-periodic behaviors, with the minimum penetration generally occurring in January, peak intensification and penetration growth occurring during late winter and spring (February to May), and maximum penetration often occurring in July [13, 14, 20]. However, it is not only the location of the LC, but also its episodic shedding of long-lived LC Eddies (LCE) that often disrupt local ecosystems and industrial operations at sea in the northern, central, and western GoM [3, 11, 18, 19, 21–32].

Scientific research, societal demands, and operational needs have driven significant progress in ocean modeling for the GoM and understanding the LC system and the GoM circulation. This includes both isolated hindcasting and forecasting studies [9, 15, 16, 18, 20, 33–44] as well as extended and

sustained forecasting operations [45–53]. The limited availability of data for these forecasting operations has led in turn to significant uncertainties in long-range modeling forecasts of the LC and LCE locations and dynamics.

For the three months of MASTR, we employed our MIT Multidisciplinary Simulation, Estimation, and Assimilation Systems (MSEAS) primitive equation (PE) submesoscale-to-regional-scale ocean modeling system [7, 54, 55], processed and assimilated multiple data types, and issued and described in real-time deterministic and probabilistic forecasts of ocean fields and derived quantities [2]. For the first time in the region, we provided daily (i) multi-resolution large-ensemble forecasts with initial conditions downscaled from two global models (HYCOM [56] and Mercator [57]) with multi-region three-dimensional (3D) PE-field perturbations using Error Subspace Statistical Estimation (ESSE), stochastic tidal and atmospheric forcing, and implicit 2-way nesting, (ii) mutual information forecasts for sampling and predictability studies, (iii) optimal adaptive sampling guidance for air and sea sensing platforms, and (iv) reachability forecasts for underwater vehicles [58].

Figure 1 highlights a few of these real-time results [2]. A forecast of optimal candidate sampling paths for Remote Ocean Current Imaging System (ROCIS) flights on February 20, 2024, is shown in figure 1a, The adaptive sampling predicts that this flight path maximizes the mutual information (MI) between the surface velocity to be measured along the flight path and the cyclonic eddies on the LC's western wall represented by the density anomaly σ_T and velocity field at a set of verification locations on February 23. Figures 1b, 1c, and 1d are forecasts for April 9, 2024: the relative vorticity field at 2 m, the 100 m σ_T field, and its standard deviation field, respectively. We highlight the surface eddies in the Caribbean Sea, the extended LC with the recently detached eddy Cardone, the currents and remnants of eddy Berek in the western Gulf, and the larger σ_T uncertainties around the LC and eddy Cardone. Figures 1e and 1f show forecast sections along the Yucatán Channel (YC) in salinity and its standard deviation for April 9. The forecasts capture the sloping subsurface salinity maximum and return flow by Cuba, and highlight the larger standard deviation on the edges of this maximum, especially on the upper edge in response to atmospheric forcing uncertainty. Figure 1g is a forecast for April 9 of the probability of the surface velocity being 1.5 kt or greater, a key metric for the GoM industry. Figure 1h compares the ensemble forecast for April 3 to a salinity data profile, many more of which confirm predictive skill up to 14 days and beating persistence [2].

The remainder of this paper is organized as follows. In section II, we outline our probabilistic ocean modeling system, including the initialization procedure, describe our adaptive sampling methodology, and summarize our reachability and path planning forecasting systems. In section III, we highlight some of our real-time deterministic and probabilistic forecast products, including their setup and real-time forecasting skill evaluation. In section IV, we present our real-time mutual information forecasts for optimal adaptive sampling guidance for sensing platforms on ROCIS flights. In section V, we present our real-time probabilistic reachability forecasts for gliders deployed and operated by the MASTR team. Finally, we summarize and conclude in section VI.

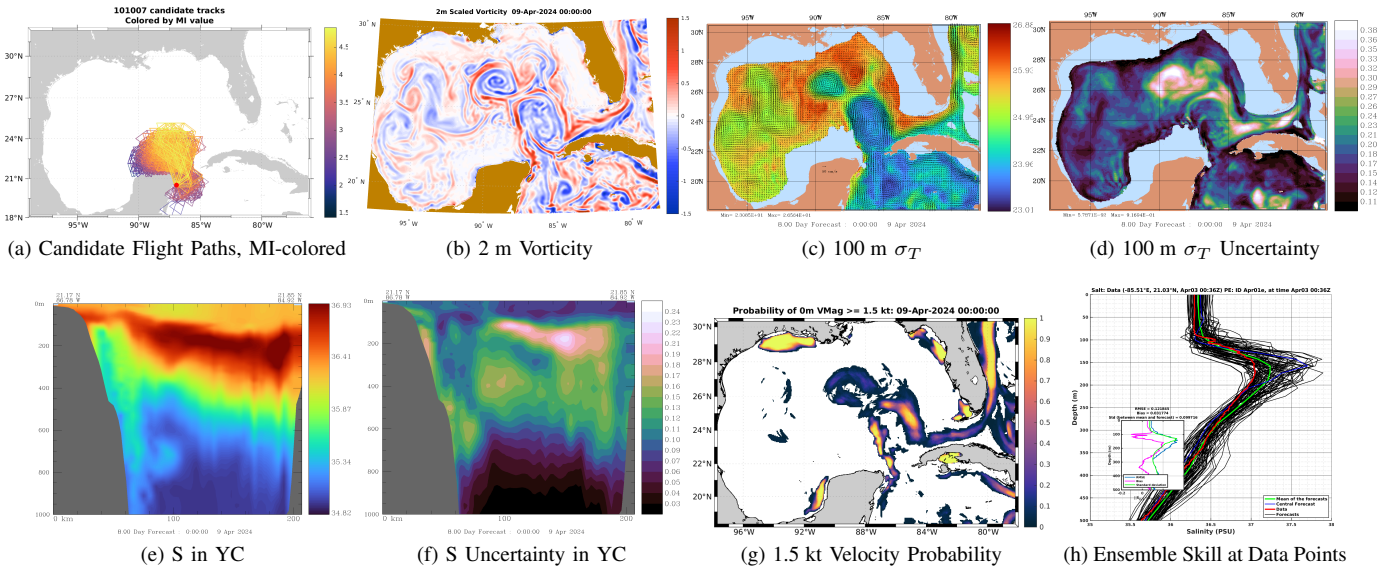

(a) Candidate Flight Paths, MI-colored (b) 2 m Vorticity (c) 100 m σ_T (d) 100 m σ_T Uncertainty

(e) S in YC (f) S Uncertainty in YC (g) 1.5 kt Velocity Probability (h) Ensemble Skill at Data Points

Fig. 1: Examples of MSEAS forecast products issued in real-time during MASTR [2]. Unless otherwise specified, all images are forecasts for April 9. (a) Candidate ROCIS flight paths for February 23, ordered and colored by the forecast mutual information (MI) about the target verification field. (b) Vorticity (scaled by f) at 2 m. (c) 100 m σ_T. (d) Uncertainty (ensemble standard deviation) in 100 m σ_T. (e) Salinity in YC. Notice that the MSEAS forecast captures the subsurface salinity maximum. (f) Uncertainty (ensemble standard deviation) in salinity in YC. Peak uncertainty aligns with the upper edge of the subsurface maximum. (g) Forecast of the probability of the surface velocity being 1.5 kt or greater. The probable high velocities are limited to the vicinity of the LC, eddies, and regions of strong tides at 00Z. (h) Ensemble skill against a salinity profile on April 3. Note that the data profile is contained within the ensemble envelope.

II. Methodology

For the large-ensemble forecasting of physical ocean fields, uncertainties, and risks, we employed our MIT MSEAS-PE and ESSE systems [54, 55, 59–62]. These systems have been used for fundamental research and for realistic simulations in varied regions of the World Ocean [63–69]. Among the capabilities of the MSEAS-PE is its ability to simulate sub-mesoscale processes over regional domains with complex geometries and varied interactions using an implicit two-way nesting/tiling scheme [54]. During MASTR, we leveraged many of our systems' capabilities, including deterministic and ensemble initialization schemes [55, 70, 71], tidal prediction and inversion [72], fast-marching coastal objective analysis [73], subgrid-scale models [74, 75], advanced data assimilation schemes [76, 77], and path planning, reachability and adaptive sampling [65, 77–79].

We initialize large ESSE forecast ensembles [75, 77, 80] with perturbed initial conditions, boundary conditions, and stochastic forcing [7, 75, 81, 82]. To create 3D PE-balanced initial ESSE perturbations, we use historical CTD profiles which we quality control and segregate into water masses. For each region, we then compute 1D vertical multivariate empirical modes. These vertical modes are combined with 2D horizontal modes created by an eigendecomposition of the horizontal correlation matrix to produce 3D temperature and salinity modes [7, 70, 71]. Perturbations of magnitude equal to a fraction of this variability are constructed from these modes for each region. They are combined based on the fronts of the deterministic initial conditions (ICs) to create 3D temperature and salinity perturbations for the entire domain. Initial perturbations for sea surface height (SSH) and velocity are obtained through geostrophy. The ESSE ensembles are forced with stochastic boundary, tidal, and atmospheric forcing.

For adaptive sampling [77, 79], we employ mutual information (MI), that is, the "amount of information" gathered by observations about the scientific objectives or variables of interest [7, 65]. For MASTR, our goal is to maximize this MI over all locations that can be reached by ROCIS flights or gliders. First, we obtain all operationally feasible sampling paths or reachable regions. Second, we use the large-ensemble MSEAS-PE forecasts to predict the MI between the scientific variables of interest and the observed variables along candidate paths. Third, we select the optimal paths. The regions an ocean vehicle can reach over time and its optimal paths to desired locations depend on ocean currents. To forecast these reachability fields and time-optimal paths for glider operations, we use exact differential equations [65, 83–87]. They are forced by ocean current forecasts and their probabilities, and integrated using level-set numerical schemes [58, 88, 89].

III. Real-time Probabilistic Forecasting

Our multi-resolution large-ensemble forecasts were of 5 to 14 days duration using 100 optimized vertical levels and 1/25° horizontal resolution (some at 1/12.5°). Initial conditions were downscaled from two global models (HYCOM and Mercator). They were forced by blended NAM 12 km and GFS $1/4°$ hourly air-sea fluxes from NCEP and by tides from TPXO8-Atlas of OSU adapted to the high-resolution bathymetry and coastlines [72]. We utilized the bathymetry from the Shuttle Radar Topography Mission (SRTM) 15-arcsecond global map [90], merged with the CICESE bathymetry for the Cozumel region. Forecast fields were issued daily and described using snapshot time-series maps, sections, and interactive visualization [91]. The data of opportunity and data from MASTR were processed and displayed (Argo float and glider CTDs, NDBC buoy data, and satellite SSH and SST), see [2]. We used these data to evaluate the skill of our forecasts in real time, computing skill metrics that compare forecasts at data points to measured values (see Sects. III-A and III-B).

To initialize the ESSE ensemble, we segregated the historical February CTD profiles (2008–2024) from the World Ocean Database [92] into the three water mass regions (Fig. 2). Horizontal correlations had a 100 km decay scale and 250 km zero-crossing. Initial velocity perturbations were computed using a 4000 m level of no motion. These perturbations were then applied to central IC/BC fields downscaled from Mercator or HYCOM. To add uncertainty to the forcings, two different atmospheric forecast products (the blended NAM/GFS described above and the pure GFS) were used with small random amplitude/phase perturbations. Similarly, 27 different versions of the fitted TPXO-8 (using different friction parameters) were employed, again with random amplitude/phase perturbations.

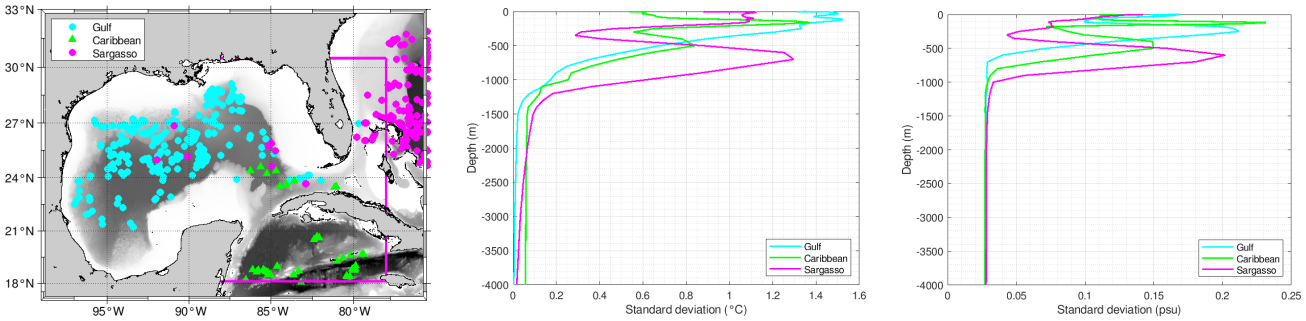

(a) Historical data locations (b) Temperature standard deviation profiles (c) Salinity standard deviation profiles

Fig. 2: Locations and standard deviation profiles of historical in situ data for February, segregated by water mass and used to construct 3D modes for the initial 3D PE-balanced ESSE perturbations.

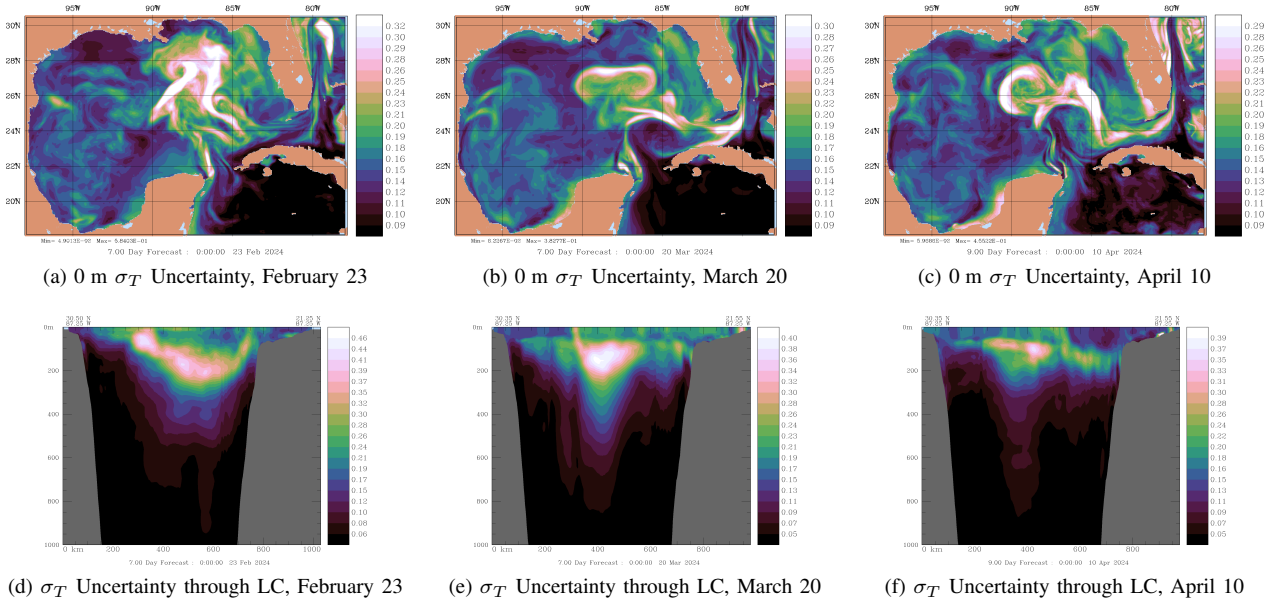

(a) 0 m σ_T Uncertainty, February 23 (b) 0 m σ_T Uncertainty, March 20 (c) 0 m σ_T Uncertainty, April 10

(d) σ_T Uncertainty through LC, February 23 (e) σ_T Uncertainty through LC, March 20 (f) σ_T Uncertainty through LC, April 10

Fig. 3: MSEAS ESSE probabilistic forecasts of standard deviation for σ_T. Top row: Standard deviation of surface σ_T for February 23, March 20, and April 10, 2024. Bottom row: As top row, but for a vertical section along 87.25°W (Florida to Yucatán, through the LC).

Figure 3 shows uncertainty forecasts in density σ_T at three periods of the MASTR experiment. On February 23, Fig. 3a and 3d, the LC was in an extended state. The greatest uncertainty surrounded the northern extent of the LC. At depth (in the 87.25°W section; Fig. 3d), there was a subsurface maximum of uncertainty starting at 100 m and down to 200 m as the LC detached from Campeche Bank. On March 20, Figs. 3b and 3e, the LC was transitioning from an extended state to a likely LCE separation. The uncertainty was maximum around the northern limit of the LC with a wider east-west extent reflecting the evolution of the future LCE. A secondary maximum occurred around 25°N, foreshadowing the future position of the LC in the separation state. At depth, Fig. 3e, the subsurface maxima occurred at the midpoint of the section, around the latitude of the future LCE separation. On April 10, Figs. 3c and 3f, LCE Cardone had been separated from the LC for about one week. The uncertainty was largest in three regions: (1) the west side of LCE Cardone, (2) along the boundary of the LC and Cardone, due to interactions in some ensemble realizations, and (3) at the eastern wall of the LC. At depth, Fig. 3f, the location of the subsurface maximum uncertainty was shallower, at 100 m, and occurred at the boundary of the LC and Cardone.

Of interest to the GoM industry are the locations of currents exceeding 1.5 kt; we provided real-time forecasts of such hazardous velocities and their statistics. Fig. 4 shows an example for February 16–20. The likelihood of hazardous velocities increases along the LC's western wall over time, and is also high in the southwest flank of eddy Berek. Winds on February 17–18 lead to higher then normal probabilities of

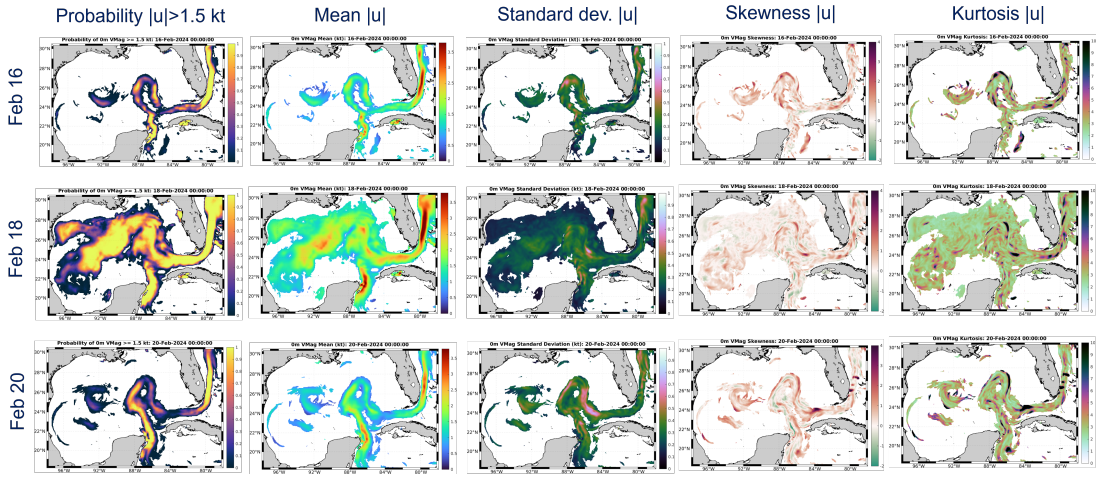

Fig. 4: Statistics of surface velocity magnitude to exceed 1.5 kt, predicted from MSEAS real-time probabilistic forecasts of hazardous velocities for February 16–20, 2024.

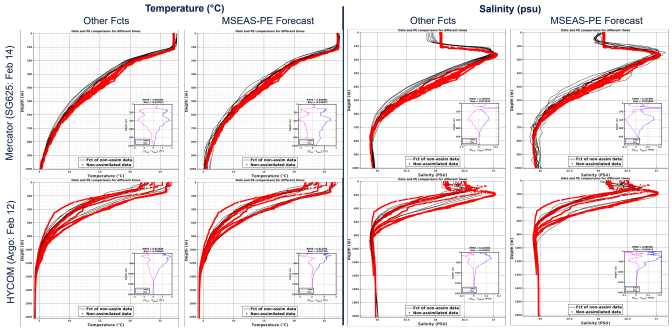

Fig. 5: MSEAS-PE deterministic forecast skill against independent T/S data. Red squares, data; black lines, model forecasts. RMSEs and biases as functions of depth are shown in the insets, along with their averaged values. Top row: Comparison of Mercator forecasts against SeaGlider 625 data on February 14 (columns 1 and 3), and comparison of MSEAS-PE forecasts initialized from downscaled Mercator against the same data (columns 2 and 4). Bottom row: As top row, but the comparison is to data from Argo on February 12.

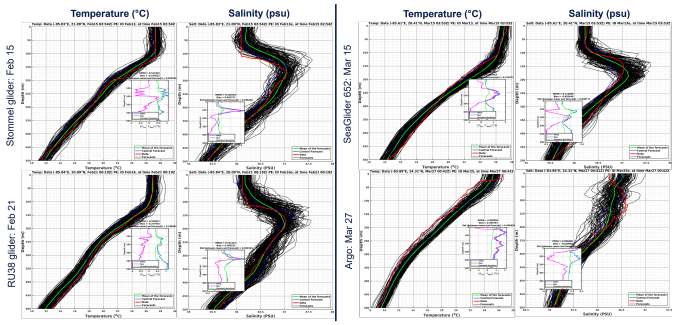

Fig. 6: MSEAS probabilistic forecast skill against independent T/S profile data from Argo floats and gliders on February 15, February 21, March 15, and March 27. Black curves are the forecasts of each ensemble member (realizations); blue curves, the central forecasts; red curves, the data; and green curves, the ensemble means.

hazardous currents throughout the LC and western Gulf. The risk of positive outliers (skewness, kurtosis) remains confined to the LC and the edges of eddy Berek. In some ESSE ensemble members, the LC almost detaches on February 20 but reattaches later (not shown).

A. *Deterministic Forecasting Skill*

Our deterministic forecasts were validated against independent data [2]. In Fig. 5, we compare the temperature and salinity from the MSEAS-PE forecasts with measurements by Argo and SeaGlider 625 on several dates. The MSEAS-PE shows skill, as the temperature and salinity profiles align well. Quantitatively, we see that the MSEAS-PE central forecasts show a reduction in RMSE of between 5% and 25% compared with the global Mercator and HYCOM forecasts.

B. *Probabilistic Forecasting Skill*

Similarly, we validated our ESSE ensemble forecasts against independent data by comparing to T/S profiles from Argo and gliders deployed by the MASTR team. In Fig. 6, we compare four different ensemble forecasts on four dates (their durations vary between 2 and 5 days). Notice that in all cases, the data profile is contained within the range of ensemble predictions at all depths, and agrees well with the ensemble mean forecast, demonstrating skill up to at least 5 days.

IV. Real-time Mutual Information Forecasts for Adaptive Sampling

One of our goals for the MASTR sea exercise was to provide optimal adaptive sampling guidance for air and sea sensing platforms using mutual information (MI) fields, or the information contained in candidate data about the ocean dynamics of interest or target fields [65, 82]. A scientific interest for MASTR was the (cyclonic) eddies near and past the YC at the western wall of the LC. Our adaptive sampling goal was thus to predict which ROCIS flight paths, and the surface velocity data they sample, provide the most information about the density anomaly σ_T and surface velocity of the (cyclonic) eddies (the target fields), at future times.

During the experiment, we forecasted the MI-optimal flight paths for many different days [2]; the components of one such forecast are shown in Fig. 7. Here, we forecast the optimal path for February 20. It will sample surface velocity on that day, whose central forecast field is shown in Fig. 7b. The goal is to predict the path on February 20 that samples surface velocity and maximizes the information content about the surface σ_T and velocity on February 23 (fields shown in Fig. 7c) at the 20 target grid-points shown in Fig. 7a. If a flight measured only a single surface velocity value, the MI field shown in Fig. 7a would allow one to select the ideal location. However, flights measure surface velocity all along their paths, hence the total MI for each flight path is needed.

The MI-optimal flight paths were forecast and selected in real-time in two steps: (i) We determined all valid paths that satisfied normal operational criteria ahead of time (e.g., constraining path length, possible bearing angles and segments, and pruning away invalid paths that leave the region, don't return to the starting airport, have too much repetition, spend too much time over land, or are duplicates), and (ii) We used the large-ensemble MSEAS-PE forecasts to predict the MI between surface currents along each valid path and the future target fields (surface values of σ_T and u, v at the 20 grid-points shown in Fig. 7a). The paths were then ranked according to their MI values and the path with the maximum MI was selected as the optimal path to complete.

The resulting candidate paths, when we target σ_T alone and thus optimize for information on the upper-layer eddies of the western wall, are shown colored by MI value in Fig. 7e; the corresponding MI histogram is shown in Fig. 7d. Of these, the path with maximal MI is shown in Fig. 7f. We find that paths with higher MI lead flights northward of Cozumel toward the western wall, as expected, that similar paths have similar MI values, and that the most informative paths usually agree with physics intuition or uncertainties (e.g., the possible presence and advection of smaller-scale eddies, and the uncertain position and strength of LCEs). Lastly, we examine the effect of the choice of verification field in Figs. 7g–7i. Here, we target

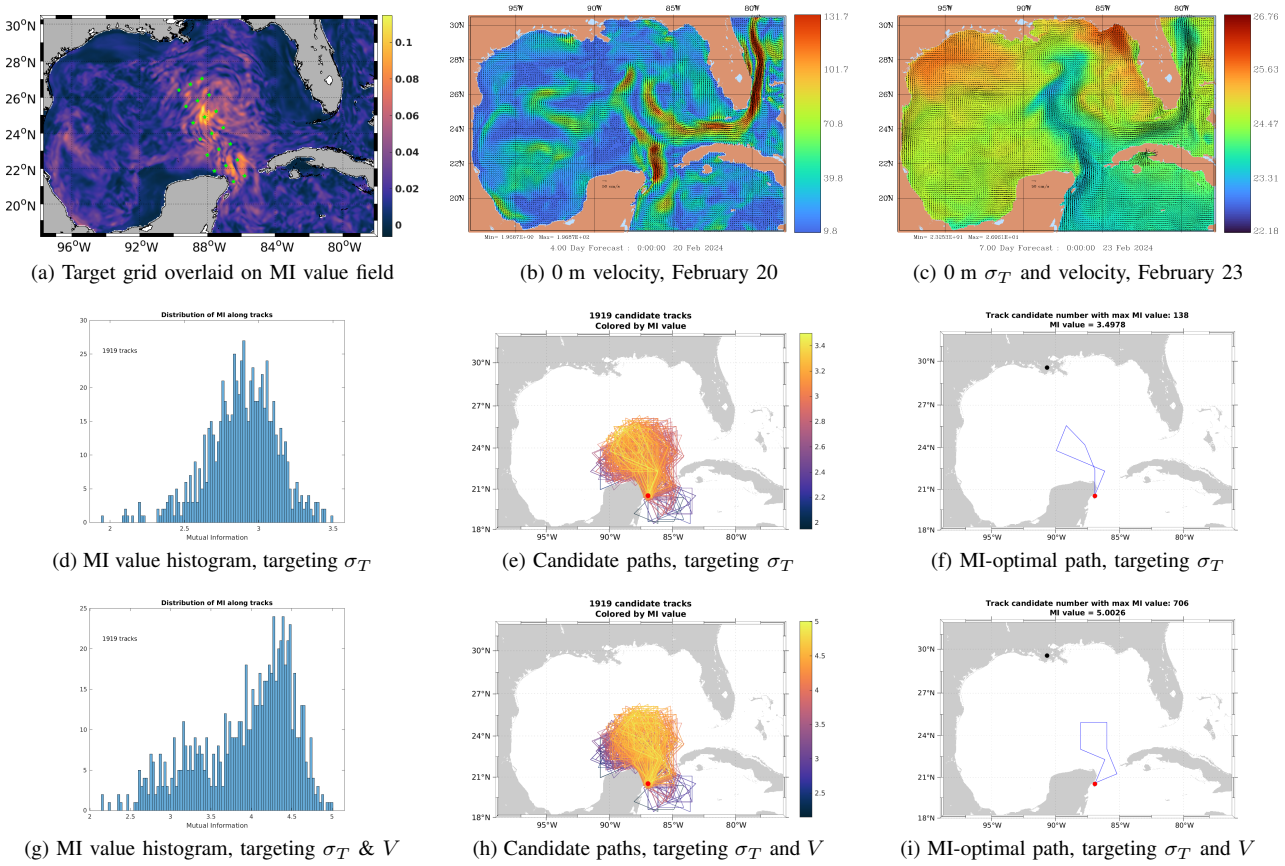

(a) Target grid overlaid on MI value field
(b) 0 m velocity, February 20
(c) 0 m σ_T and velocity, February 23
(d) MI value histogram, targeting σ_T
(e) Candidate paths, targeting σ_T
(f) MI-optimal path, targeting σ_T
(g) MI value histogram, targeting σ_T & V
(h) Candidate paths, targeting σ_T and V
(i) MI-optimal path, targeting σ_T and V

Fig. 7: Real-time forecasts of MI-optimal ROCIS flight paths which start and end at Cozumel. All paths are constrained to be 800 nmi in length and contain 16 possible bearing angles and 7 segments. The flight (measurement) date is February 20; the verification (target) date is February 23. All panels show MSEAS forecasts: (a) Verification grid (20 points) covering the LC western wall and associated eddies, overlaid on the MI field between each surface velocity and the σ_T values at all verification grid-points; (b) 0 m velocity on February 20; (c) 0 m σ_T, with velocity overlaid, on February 23; (d) MI value histogram, targeting σ_T alone; (e) Candidate paths, ordered and colored by forecast MI about σ_T alone; (f) MI-optimal path for a flight on February 20 optimized for σ_T on February 23; (g–i) As (d–f), respectively, but targeting both σ_T and velocity.

both σ_T and velocity, and are interested in both the upper-layer eddies of the western wall and the full LC flow. The results then show an eastward shift and widening of the MI-optimal flight path, covering the western wall (Figs. 7i).

V. Real-time Reachability Forecasts

Our large-scale ensemble forecasts were used to forecast deterministic and probabilistic reachable regions for marine platforms. Details of this forecasting can be found in [58].

The MSEAS probabilistic reachability forecast for March 28 to April 3 is shown in Fig. 8. Ensemble means of 0–1000 m averaged velocity are shown in Figs. 8a–d. Near the YC, the larger mean currents (more than 30 cm/s) were in two main areas. The first was by the Yucatán Peninsula (YP) north of Cozumel, where a northward flow is increasing during this period. The second was by the western tip of Cuba, where a decreasing southward flow occurred. Figs. 8e–h show ensemble standard deviations of the 0–1000 m averaged currents. Uncertainty was minimal by the YP south of Cozumel, but larger to the east (in the Caribbean) and grew over time in this region. It was also larger north of Cozumel, especially between March 28 and March 30. Figs. 8i–l show the probability of glider RU38 reaching any point starting from around 18.75°N, 86.4°W at 0Z on March 26, with an assumed propulsion speed of 40 cm/s. The reachability front initially distorts westward by the local mean flow and later stretches northward when it reaches the high currents north of Cozumel. Initially, the transition zone from certain reachability (probability 1) to unreachable (probability 0) is much narrower on the west (near the YP), reflecting the lower uncertainty there. Lastly, Figs. 8m–p show the probability of the Stommel glider reaching any point starting from around 21.55°N, 85.2°W at 0Z on March 26, with an assumed speed of 30 cm/s. This reachability front first grows southward and then eastward, in accord with an eddy and currents south of Cuba. Later, it distorts to the northwest following the northward LC around the YP. The transition zone from certain reachability to unreachable is fairly uniform, with some narrowing near Cuba.

VI. Conclusions

For MASTR during February–April 2024, we applied MSEAS systems in real time to provide large-ensemble ocean

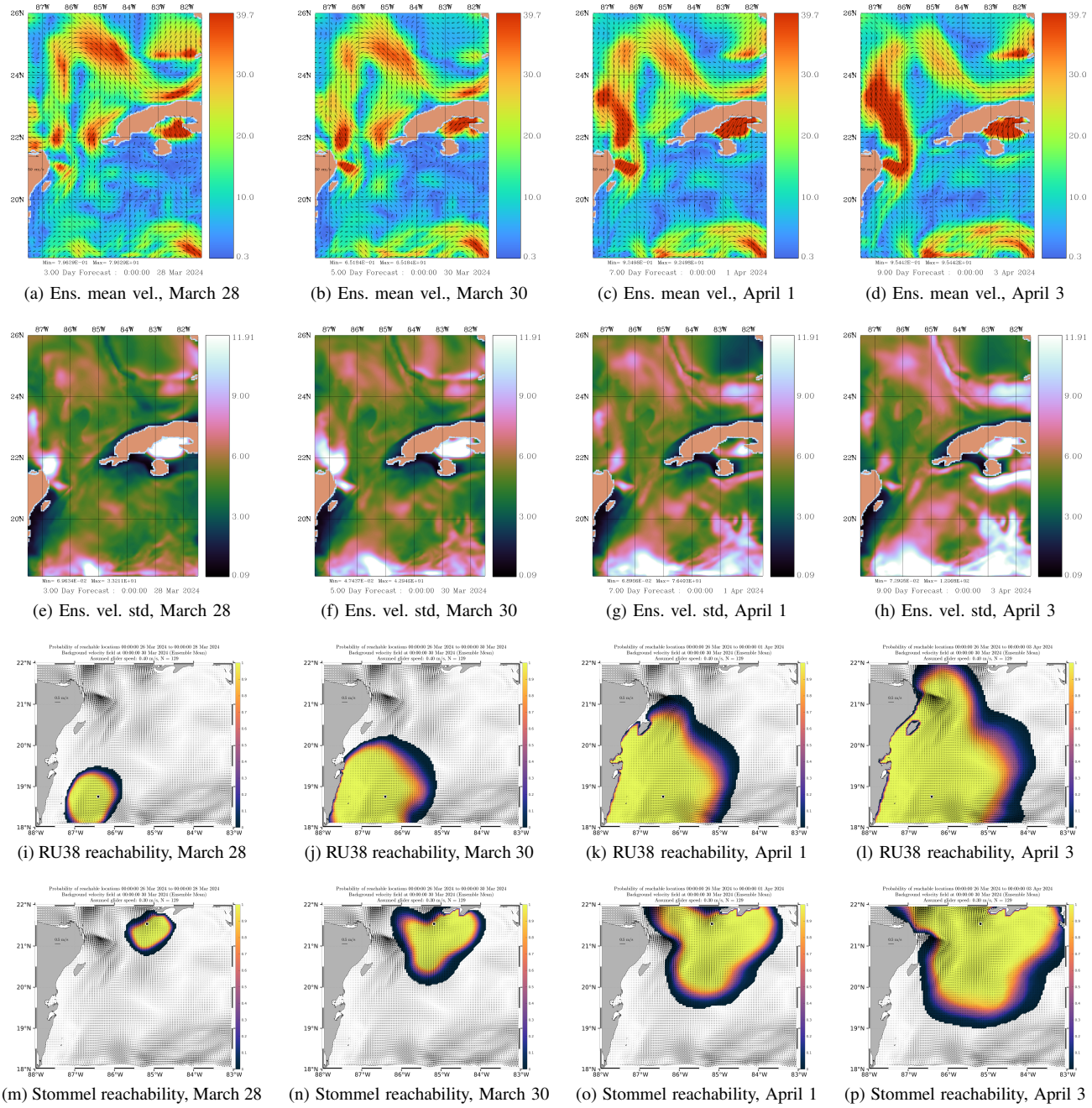

(a) Ens. mean vel., March 28 (b) Ens. mean vel., March 30 (c) Ens. mean vel., April 1 (d) Ens. mean vel., April 3

(e) Ens. vel. std, March 28 (f) Ens. vel. std, March 30 (g) Ens. vel. std, April 1 (h) Ens. vel. std, April 3

(i) RU38 reachability, March 28 (j) RU38 reachability, March 30 (k) RU38 reachability, April 1 (l) RU38 reachability, April 3

(m) Stommel reachability, March 28 (n) Stommel reachability, March 30 (o) Stommel reachability, April 1 (p) Stommel reachability, April 3

Fig. 8: MSEAS 0–1000 m averaged velocity ensemble mean and standard deviation and probabilistic glider reachability forecasts from March 28 to April 3. The assumed speed for RU38 is 40;cm/s; for Stommel, 30 cm/s. The final two rows show the probability that the glider can reach any point by the indicated date from its position at 0Z on March 26: Yellow regions indicate certain reachability (probability 1); white regions are unreachable (probability 0).

forecasts, predict reachable sets and optimal paths for gliders, and guide sampling aircraft and ocean vehicles toward the most informative observations. Our ocean ICs were downscaled from two global models and data-corrected. The ensemble forecasts employed multi-region data-driven balanced initialization, random model parameters, and stochastic boundary, tidal, and atmospheric forcing. Deterministic and large-ensemble probabilistic forecasts of the LC state, LCEs Berek and Cardone, and overall circulation in the GoM were issued, demonstrating predictive skill when compared to independent data. We predicted statistics and PDFs of hazardous currents, showing that the highest risks of positive outliers were confined to the LC and eddies while wind events could lead to hazardous currents throughout the LC and western Gulf. We issued MI forecasts for adaptive sampling for air and sea sensing platforms, using varied target fields, dates, and path constraints. Multivariate MI-optimal flight paths for the LC western wall and its eddies were consistent with dynamics

and varied with measurement and verification times, target variables, path length, and path complexity (number of allowed segments, bearing angles, and so on). Lastly, we issued probabilistic reachability forecasts for gliders highlighting the links between uncertain currents and the likelihood of reachable locations. All these results are promising for future GoM studies and the GoM stakeholders.

ACKNOWLEDGMENTS

We thank all members of the MIT-MSEAS group and all of our Gulf of Mexico colleagues. We also thank the HYCOM Consortium and Mercator Ocean for their ocean model fields, and Matthew Pyle, Eric Rogers, Geoff DiMego, and Arun Chawla of NCEP for their atmospheric forecasts. We acknowledge support from the Gulf Research Program of the National Academies of Sciences, Engineering, and Medicine under award number 2000013149. The content is solely the responsibility of the authors and does not necessarily represent the official views of the Gulf Research Program or the National Academies of Sciences, Engineering, and Medicine.

REFERENCES

[1] S. F. DiMarco *et al.*, "Applications of adaptive sampling strategies of autonomous vehicles, drifters, floats, and HF-radar, to improve Loop Current system dynamics forecasts in the deepwater Gulf of Mexico," in *Offshore Technology Conference*. OTC, 2023, p. D031S035R005.

[2] MSEAS MASTR Ex., "MASTR Real-time Gulf of Mexico Sea Experiment 2024: Gulf of Mexico – February–April, 2024," Apr. 2024. [Online]. Available: http://mseas.mit.edu/Sea_exercises/GOFFISH/MASTR/

[3] The National Academy of Sciences, "Understanding Gulf ocean systems," 2018. [Online]. Available: https://www.nationalacademies.org/gulf/fellowships-and-grants/understanding-gulf-ocean-systems

[4] M. Cadwaller, "Eddy Lazarus & the Loop Current – paralyzing the Gulf in 2014," American Association of Drilling Engineers: Innovative and Emerging Technology Study Group, 2015.

[5] S. F. DiMarco, W. D. Nowlin, and R. Reid, "A statistical description of the velocity fields from upper ocean drifters in the Gulf of Mexico," *Geophysical Monograph-American Geophysical Union*, vol. 161, p. 101, 2005.

[6] A. K. Nickerson, R. H. Weisberg, and Y. Liu, "On the evolution of the Gulf of Mexico Loop Current through its penetrative, ring shedding and retracted states," *Advances in Space Research*, vol. 69, no. 11, pp. 4058–4077, 2022.

[7] P. J. Haley, Jr., C. Mirabito, M. Doshi, and P. F. J. Lermusiaux, "Ensemble forecasting for the Gulf of Mexico Loop Current region," in *OCEANS 2023 IEEE/MTS Gulf Coast*. Biloxi, MS: IEEE, Sep. 2023.

[8] A. Alvera-Azcárate, A. Barth, and R. H. Weisberg, "The surface circulation of the Caribbean Sea and the Gulf of Mexico as inferred from satellite altimetry," *Journal of Physical Oceanography*, vol. 39, no. 3, pp. 640–657, 2009.

[9] G. Gopalakrishnan, B. D. Cornuelle, I. Hoteit, D. L. Rudnick, and W. B. Owens, "State estimates and forecasts of the loop current in the Gulf of Mexico using the MITgcm and its adjoint," *Journal of Geophysical Research: Oceans*, vol. 118, no. 7, pp. 3292–3314, 2013.

[10] P. Hamilton *et al.*, "Observations and dynamics of the Loop Current," US Department of the Interior, Bureau of Ocean Energy Management, Gulf of Mexico OCS Region, New Orleans, OCS Study BOEM 2015-006, 2014.

[11] X. Zeng, Y. Li, and R. He, "Predictability of the loop current variation and eddy shedding process in the Gulf of Mexico using an artificial neural network approach," *Journal of Atmospheric and Oceanic Technology*, vol. 32, no. 5, pp. 1098–1111, 2015.

[12] G. Manta, G. Durante, J. Candela, U. Send, J. Sheinbaum, M. Lankhorst, and R. Laxenaire, "Predicting the loop current dynamics combining altimetry and deep flow measurements through the yucatan channel," *Frontiers in Marine Science*, vol. 10, 2023.

[13] D. W. Behringer, R. L. Molinari, and J. F. Festa, "The variability of anticyclonic current patterns in the Gulf of Mexico," *Journal of Geophysical Research*, vol. 82, no. 34, pp. 5469–5476, 1977.

[14] F. M. Vukovich, "Loop current boundary variations," *Journal of Geophysical Research: Oceans*, vol. 93, no. C12, pp. 15 585–15 591, 1988.

[15] G. Gopalakrishnan, B. D. Cornuelle, and I. Hoteit, "Adjoint sensitivity studies of loop current and eddy shedding in the Gulf of Mexico," *Journal of Geophysical Research: Oceans*, vol. 118, no. 7, pp. 3315–3335, 2013.

[16] D. S. Dukhovskoy *et al.*, "Characterization of the uncertainty of loop current metrics using a multidecadal numerical simulation and altimeter observations," *Deep Sea Research Part I*, vol. 100, pp. 140–158, 2015.

[17] J. Sheinbaum, G. Athié, J. Candela, J. Ochoa, and A. Romero-Arteaga, "Structure and variability of the Yucatan and loop currents along the slope and shelf break of the Yucatan channel and Campeche bank," *Dynamics of Atmospheres and Oceans*, vol. 76, pp. 217–239, 2016.

[18] J. Jouanno *et al.*, "Loop Current frontal eddies: Formation along the Campeche Bank and impact of coastally trapped waves," *Journal of Physical Oceanography*, vol. 46, no. 11, pp. 3339–3363, 2016.

[19] H. Furey, A. Bower, P. Perez-Brunius, P. Hamilton, and R. Leben, "Deep eddies in the Gulf of Mexico observed with floats," *Journal of Physical Oceanography*, vol. 48, no. 11, pp. 2703–2719, 2018.

[20] A. Lugo-Fernández, "Modeling the intrusion of the Loop Current into the Gulf of Mexico," *Dynamics of Atmospheres and Oceans*, vol. 84, pp. 46–54, 2018.

[21] A. Lugo-Fernández and R. R. Leben, "On the linear relationship between Loop Current retreat latitude and eddy separation period," *Journal of Physical Oceanography*, vol. 40, no. 12, pp. 2778–2784, 2010.

[22] D. L. Rudnick, G. Gopalakrishnan, and B. D. Cornuelle, "Cyclonic eddies in the Gulf of Mexico: Observations by underwater gliders and simulations by numerical model," *Journal of Physical Oceanography*, vol. 45, no. 1, pp. 313 – 326, 2015.

[23] K. Donohue *et al.*, "Gulf of Mexico Loop Current path variability," *Dynamics of Atmospheres and Oceans*, vol. 76, pp. 174–194, 2016.

[24] N. Sharma, J. S. Storie, K. M. Obenour, M. J. Leber, and A. Srinivasan, "Loop Current hyperactivity: Analysis of in situ measurements in the Gulf of Mexico," in *Offshore Technology Conference*, no. OTC-27229-MS. Houston: OnePetro, May 2016, pp. 1–30.

[25] P. Hamilton, A. Bower, H. Furey, R. Leben, and P. Pérez-Brunius, "The Loop Current: Observations of deep eddies and topographic waves," *Journal of Physical Oceanography*, vol. 49, no. 6, pp. 1463 – 1483, 2019.

[26] W. Sturges and R. Leben, "Frequency of ring separations from the Loop Current in the Gulf of Mexico: A revised estimate," *Journal of Physical Oceanography*, vol. 30, no. 7, pp. 1814–1819, 2000.

[27] A. R. Johnson, K. A. Donohue, D. R. Watts, K. L. Tracey, and M. A. Kennelly, "Generation of high-frequency topographic Rossby waves in the Gulf of Mexico," *Frontiers in Marine Science*, vol. 9, 2022.

[28] E. R. Olvera-Prado, R. Romero-Centeno, J. Zavala-Hidalgo, E. Moreles, and A. Ruiz-Angulo, "Contribution of the wind, Loop Current Eddies, and topography to the circulation in the southern Gulf of Mexico," *Ocean Dynamics*, vol. 73, no. 10, pp. 597–618, 2023.

[29] E. Steele, S. Jaramillo, R. Neal, J. Storie, and X. Zhang, "Prediction of Loop Current and Eddy Regimes in the Gulf of Mexico," in *OTC Offshore Technology Conference*, vol. 3, 2023, p. D031S035R006.

[30] J. Storie *et al.*, "Evaluation of Loop Current/Loop Current Eddy Fronts to Guide Offshore Oil and Gas Operations," in *OTC Offshore Technology Conference*, vol. 3, 2023, p. D031S035R002.

[31] E. R. Olvera-Prado, S. L. Morey, and E. P. Chassignet, "Contribution of the wind and loop current eddies to the circulation in the western gulf of mexico," *Frontiers in Marine Science*, vol. 11, 2024.

[32] M. Gentil *et al.*, "Distribution, mixing, and transformation of a Loop Current ring waters: The case of Gulf of Mexico," *ESS Open Archive*, 2024.

[33] H. E. Hurlburt and J. D. Thompson, "A numerical study of Loop Current intrusions and eddy shedding," *Journal of Physical Oceanography*, vol. 10, no. 10, pp. 1611–1651, 1980.

[34] L. Oey, T. Ezer, and H. Lee, "Loop Current, rings and related circulation in the Gulf of Mexico: A review of numerical models and future challenges," in *Circulation in the Gulf of Mexico: Observations and Models*, ser. Geophysical Monograph, W. Sturges and A. Lugo-Fernandez, Eds. Washington: AGU American Geophysical Union, 2005, vol. 161, pp. 31–56.

[35] L.-Y. Oey *et al.*, "An exercise in forecasting loop current and eddy frontal positions in the Gulf of Mexico," *Geophysical Research Letters*, vol. 32, no. 12, 2005.

[36] I. Hoteit *et al.*, "A MITgcm/DART ensemble analysis and prediction system with application to the Gulf of Mexico," *Dynamics of Atmospheres and Oceans*, vol. 63, pp. 1–23, 2013.

[37] F.-H. Xu, L.-Y. Oey, Y. Miyazawa, and P. Hamilton, "Hindcasts and forecasts of Loop Current and eddies in the Gulf of Mexico using local ensemble transform Kalman filter and optimum-interpolation assimilation schemes," *Ocean Modelling*, vol. 69, pp. 22–38, 2013.

[38] J. Jouanno, E. Pallàs-Sanz, and J. Sheinbaum, "Variability and dynamics of the Yucatan upwelling: High-resolution simulations," *Journal of Geophysical Research: Oceans*, vol. 123, no. 2, pp. 1251–1262, 2018.

[39] K. Chen *et al.*, "Data assimilative modeling investigation of Gulf Stream Warm Core Ring interaction with continental shelf and slope circulation," *Journal of Geophysical Research: Oceans*, vol. 119, no. 9, pp. 5968–5991, 2014.

[40] S. L. Morey, J. Zavala-Hidalgo, and J. J. O'Brien, *The Seasonal Variability of Continental Shelf Circulation in the Northern and Western Gulf of Mexico from a High-Resolution Numerical Model*. AGU, 2005, pp. 203–218.

[41] D. S. Dukhovskoy, E. P. Chassignet, A. Bozec, and S. L. Morey, "Assessment of predictability of the Loop Current in the Gulf of Mexico from observing system experiments and observing system simulation experiments," *Frontiers in Marine Science*, vol. 10, 2023.

[42] R. Laxenaire, E. P. Chassignet, D. S. Dukhovskoy, and S. L. Morey, "Impact of upstream variability on the Loop Current dynamics in numerical simulations of the Gulf of Mexico," *Frontiers in Marine Science*, vol. 10, 2023.

[43] X. Yang, M. Le Hénaff, B. Mapes, and M. Iskandarani, "Dynamical interactions between Loop Current and Loop Current frontal eddies in a HYCOM ensemble of the circulation in the Gulf of Mexico," *Frontiers in Marine Science*, vol. 10, 2023.

[44] N. Chaichitehrani and R. He, "Investigation of ocean environmental variables and their variations associated with major Loop Current eddy-shedding events in the Gulf of Mexico," *Deep Sea Research Part II*, vol. 213, p. 105354, 2024.

[45] E. P. Chassignet *et al.*, "The HYCOM (HYbrid Coordinate Ocean Model) data assimilative system," *Journal of Marine Systems*, vol. 65, no. 1, pp. 60–83, 2007, marine Environmental Monitoring and Prediction.

[46] ——, "US GODAE: Global ocean prediction with the HYbrid Coordinate Ocean Model (HYCOM)," *Oceanography*, vol. 22, no. 2, pp. 64–75, 2009.

[47] E. J. Metzger *et al.*, "US Navy operational global ocean and Arctic ice prediction systems," *Oceanography*, vol. 27, no. 3, pp. 32–43, 2014.

[48] M. Wei *et al.*, "The performance of the US Navy's RELO ensemble, NCOM, HYCOM during the period of GLAD at-sea experiment in the Gulf of Mexico," *Deep Sea Research Part II*, vol. 129, pp. 374–393, 2016.

[49] B. C. Davis and E. A. McDonald, "Meeting the needs of southeastern coastal resource managers through coastal ocean observing systems," NOAA, SCSGC-T 06-001, 2006.

[50] Z. Xue *et al.*, "An integrated ocean circulation, wave, atmosphere, and marine ecosystem prediction system for the South Atlantic Bight and Gulf of Mexico," *Journal of Operational Oceanography*, vol. 8, no. 1, pp. 80–91, 2015.

[51] J. B. Zambon and R. He, "Development of the Coupled Northwest Atlantic Prediction System (CNAPS)," in *American Geophysical Union*, 2016, pp. PO14B–2775.

[52] Y. Liu *et al.*, "Coastal Ocean Response to Hurricane Ian as Simulated by the WFCOM and TBCOM Nowcast/Forecast Systems," in *AGU Fall Meeting Abstracts*, 2022, pp. NH43C–05.

[53] A. Srinivasan *et al.*, "A statistical interpolation code for ocean analysis and forecasting," *Journal of Atmospheric and Oceanic Technology*, vol. 39, no. 3, pp. 367–386, 2022.

[54] P. J. Haley, Jr. and P. F. J. Lermusiaux, "Multiscale two-way embedding schemes for free-surface primitive equations in the "Multidisciplinary Simulation, Estimation and Assimilation System"," *Ocean Dynamics*, vol. 60, no. 6, pp. 1497–1537, Dec. 2010.

[55] P. J. Haley, Jr., A. Agarwal, and P. F. J. Lermusiaux, "Optimizing velocities and transports for complex coastal regions and archipelagos," *Ocean Modelling*, vol. 89, pp. 1–28, May 2015.

[56] The HYCOM Consortium, "HYbrid Coordinate Ocean Model (HYCOM)," Jul. 2023, accessed 2019-04-09. [Online]. Available: https://hycom.org

[57] Mercator Ocean International, "Operational Mercator global ocean analysis and forecast," Dataset, 2024.

[58] E. M. Mule, P. J. Haley, Jr., C. Mirabito, P. F. J. Lermusiaux *et al.*, "Real-time probabilistic reachability forecasting for gliders in the Gulf of Mexico," in *OCEANS 2024 IEEE/MTS Halifax*. Halifax: IEEE, Sep. 2024, in press.

[59] P. F. J. Lermusiaux and A. R. Robinson, "Data assimilation via Error Subspace Statistical Estimation, part I: Theory and schemes," *Monthly Weather Review*, vol. 127, no. 7, pp. 1385–1407, 1999.

[60] P. F. J. Lermusiaux, "Data assimilation via Error Subspace Statistical Estimation, part II: Mid-Atlantic Bight shelfbreak front simulations, and ESSE validation," *Monthly Weather Review*, vol. 127, no. 7, pp. 1408–1432, Jul. 1999.

[61] P. F. J. Lermusiaux, P. J. Haley, W. G. Leslie, A. Agarwal, O. Logutov, and L. J. Burton, "Multiscale physical and biological dynamics in the Philippine Archipelago: Predictions and processes," *Oceanography*, vol. 24, no. 1, pp. 70–89, 2011, Special Issue on the Philippine Straits Dynamics Experiment.

[62] P. F. J. Lermusiaux, C. Mirabito, P. J. Haley, Jr., W. H. Ali, A. Gupta, S. Jana, E. Dorfman, A. Laferriere, A. Kofford, G. Shepard, M. Goldsmith, K. Heaney, E. Coelho, J. Boyle, J. Murray, L. Freitag, and A. Morozov, "Real-time probabilistic coupled ocean physics-acoustics forecasting and data assimila-

tion for underwater GPS," in *OCEANS 2020 IEEE/MTS*. IEEE, Oct. 2020, pp. 1–9.

[63] W. G. Leslie, A. R. Robinson, P. J. Haley, Jr, O. Logutov, P. A. Moreno, P. F. J. Lermusiaux, and E. Coelho, "Verification and training of real-time forecasting of multi-scale ocean dynamics for maritime rapid environmental assessment," *Journal of Marine Systems*, vol. 69, no. 1, pp. 3–16, 2008.

[64] P. J. Haley, Jr., P. F. J. Lermusiaux, A. R. Robinson, W. G. Leslie, O. Logoutov, G. Cossarini, X. S. Liang, P. Moreno, S. R. Ramp, J. D. Doyle, J. Bellingham, F. Chavez, and S. Johnston, "Forecasting and reanalysis in the Monterey Bay/California Current region for the Autonomous Ocean Sampling Network-II experiment," *Deep Sea Research Part II: Topical Studies in Oceanography*, vol. 56, no. 3–5, pp. 127–148, Feb. 2009.

[65] P. F. J. Lermusiaux, D. N. Subramani, J. Lin, C. S. Kulkarni, A. Gupta, A. Dutt, T. Lolla, P. J. Haley, Jr., W. H. Ali, C. Mirabito, and S. Jana, "A future for intelligent autonomous ocean observing systems," *Journal of Marine Research*, vol. 75, no. 6, pp. 765–813, Nov. 2017, the Sea. Volume 17, The Science of Ocean Prediction, Part 2.

[66] D. N. Subramani, P. J. Haley, Jr., and P. F. J. Lermusiaux, "Energy-optimal path planning in the coastal ocean," *Journal of Geophysical Research: Oceans*, vol. 122, pp. 3981–4003, 2017.

[67] C. S. Kulkarni, P. J. Haley, Jr., P. F. J. Lermusiaux, A. Dutt, A. Gupta, C. Mirabito, D. N. Subramani, S. Jana, W. H. Ali, T. Peacock, C. M. Royo, A. Rzeznik, and R. Supekar, "Real-time sediment plume modeling in the Southern California Bight," in *OCEANS Conference 2018*. Charleston, SC: IEEE, Oct. 2018.

[68] A. Gupta, P. J. Haley, D. N. Subramani, and P. F. J. Lermusiaux, "Fish modeling and Bayesian learning for the Lakshadweep Islands," in *OCEANS 2019 MTS/IEEE SEATTLE*. Seattle: IEEE, Oct. 2019, pp. 1–10.

[69] P. F. J. Lermusiaux, M. Doshi, C. S. Kulkarni, A. Gupta, P. J. Haley, Jr., C. Mirabito, F. Trotta, S. J. Levang, G. R. Flierl, J. Marshall, T. Peacock, and C. Noble, "Plastic pollution in the coastal oceans: Characterization and modeling," in *OCEANS 2019 MTS/IEEE SEATTLE*. Seattle: IEEE, Oct. 2019, pp. 1–10.

[70] P. F. J. Lermusiaux, D. G. M. Anderson, and C. J. Lozano, "On the mapping of multivariate geophysical fields: Error and variability subspace estimates," *Quarterly Journal of the Royal Meteorological Society*, vol. 126, no. 565, pp. 1387–1429, 2000.

[71] P. F. J. Lermusiaux, "On the mapping of multivariate geophysical fields: Sensitivities to size, scales, and dynamics," *Journal of Atmospheric and Oceanic Technology*, vol. 19, no. 10, pp. 1602–1637, 2002.

[72] O. G. Logutov and P. F. J. Lermusiaux, "Inverse barotropic tidal estimation for regional ocean applications," *Ocean Modelling*, vol. 25, no. 1–2, pp. 17–34, 2008. [Online]. Available: http://www.sciencedirect.com/science/article/pii/S1463500308000851

[73] A. Agarwal and P. F. J. Lermusiaux, "Statistical field estimation for complex coastal regions and archipelagos," *Ocean Modelling*, vol. 40, no. 2, pp. 164–189, 2011.

[74] P. F. J. Lermusiaux, "Evolving the subspace of the three-dimensional multiscale ocean variability: Massachusetts Bay," *Journal of Marine Systems*, vol. 29, no. 1, pp. 385–422, 2001.

[75] P. F. J. Lermusiaux, "Uncertainty estimation and prediction for interdisciplinary ocean dynamics," *Journal of Computational Physics*, vol. 217, no. 1, pp. 176–199, 2006.

[76] P. F. J. Lermusiaux, "Estimation and study of mesoscale variability in the Strait of Sicily," *Dynamics of Atmospheres and Oceans*, vol. 29, no. 2, pp. 255–303, 1999.

[77] P. F. J. Lermusiaux, "Adaptive modeling, adaptive data assimilation and adaptive sampling," *Physica D: Nonlinear Phenomena*, vol. 230, no. 1, pp. 172–196, 2007.

[78] P. F. J. Lermusiaux, T. Lolla, P. J. Haley, Jr., K. Yigit, M. P. Ueckermann, T. Sondergaard, and W. G. Leslie, "Science of autonomy: Time-optimal path planning and adaptive sampling for swarms of ocean vehicles," in *Springer Handbook of Ocean Engineering: Autonomous Ocean Vehicles, Subsystems and Control*, T. Curtin, Ed. Springer, 2016, ch. 21, pp. 481–498.

[79] P. F. J. Lermusiaux, P. J. Haley, Jr, and N. K. Yilmaz, "Environmental prediction, path planning and adaptive sampling: Sensing and modeling for efficient ocean monitoring, management and pollution control," *Sea Technology*, vol. 48, no. 9, pp. 35–38, 2007.

[80] P. F. J. Lermusiaux, A. J. Miller, and N. Pinardi, "Special issue of Dynamics of Atmospheres and Oceans in honor of Prof. A. R. Robinson," *Dynamics of Atmospheres and Oceans*, vol. 52, no. 1–2, pp. 1–3, Sep. 2011, Editorial.

[81] P. F. J. Lermusiaux, P. Malanotte-Rizzoli, D. Stammer, J. Carton, J. Cummings, and A. M. Moore, "Progress and prospects of U.S. data assimilation in ocean research," *Oceanography*, vol. 19, no. 1, pp. 172–183, 2006.

[82] P. F. J. Lermusiaux, P. J. Haley, Jr., S. Jana, A. Gupta, C. S. Kulkarni, C. Mirabito, W. H. Ali, D. N. Subramani, A. Dutt, J. Lin, A. Shcherbina, C. Lee, and A. Gangopadhyay, "Optimal planning and sampling predictions for autonomous and Lagrangian platforms and sensors in the northern Arabian Sea," *Oceanography*, vol. 30, no. 2, pp. 172–185, Jun. 2017, special issue on Autonomous and Lagrangian Platforms and Sensors (ALPS).

[83] T. Lolla, P. F. J. Lermusiaux, M. P. Ueckermann, and P. J. Haley, Jr., "Time-optimal path planning in dynamic flows using level set equations: Theory and schemes," *Ocean Dynamics*, vol. 64, no. 10, pp. 1373–1397, 2014.

[84] T. Lolla, P. J. Haley, Jr., and P. F. J. Lermusiaux, "Path planning in multiscale ocean flows: Coordination and dynamic obstacles," *Ocean Modelling*, vol. 94, pp. 46–66, 2015.

[85] D. N. Subramani, Q. J. Wei, and P. F. J. Lermusiaux, "Stochastic time-optimal path-planning in uncertain, strong, and dynamic flows," *Computer Methods in Applied Mechanics and Engineering*, vol. 333, pp. 218–237, 2018.

[86] D. N. Subramani and P. F. J. Lermusiaux, "Risk-optimal path planning in stochastic dynamic environments," *Computer Methods in Applied Mechanics and Engineering*, vol. 353, pp. 391–415, Aug. 2019.

[87] M. Doshi, M. Bhabra, M. Wiggert, C. J. Tomlin, and P. F. J. Lermusiaux, "Hamilton–Jacobi multi-time reachability," in *2022 IEEE 61st Conference on Decision and Control (CDC)*, Cuncún, Mexico, Dec. 2022, pp. 2443–2450.

[88] T. Lolla, M. P. Ueckermann, K. Yiğit, P. J. Haley, Jr., and P. F. J. Lermusiaux, "Path planning in time dependent flow fields using level set methods," in *IEEE International Conference on Robotics and Automation (ICRA), 14-18 May 2012*, 2012, pp. 166–173.

[89] C. S. Kulkarni and P. F. J. Lermusiaux, "Three-dimensional time-optimal path planning in the ocean," *Ocean Modelling*, vol. 152, Aug. 2020.

[90] B. Tozer *et al.*, "Global bathymetry and topography at 15 arc sec: SRTM15+," *Earth and Space Science*, vol. 6, no. 10, pp. 1847–1864, 2019.

[91] W. H. Ali, M. H. Mirhi, A. Gupta, C. S. Kulkarni, C. Foucart, M. M. Doshi, D. N. Subramani, C. Mirabito, P. J. Haley, Jr., and P. F. J. Lermusiaux, "Seavizkit: Interactive maps for ocean visualization," in *OCEANS 2019 MTS/IEEE SEATTLE*. Seattle: IEEE, Oct. 2019, pp. 1–10.

[92] T. P. Boyer *et al.*, *World Ocean Database 2018*, NOAA, Silver Spring, MD, 2018.